Superconducting microcircuit and fluxoid quantization: A new quantum interferometer

H. J. Fink, J. Loo,* and S. M. Roberts†
Department of Electrical Engineering and Computer Science, University of California, Davis, Davis, California 95616
(Received 21 July 1987)

Detailed solutions of the nonlinear Ginzburg-Landau equations are presented for a superconducting ring connected to two long leads. We assume a homogeneous wire of transverse dimension smaller than the coherence length ξ and penetration depth λ. This circuit behaves in much the same way as an ordinary superconducting quantum-interference device when the ring diameter is of order of magnitude of $\xi(t)$, even though it contains no Josephson junctions. The normal-superconducting phase boundary of this device can be shifted with temperature and thus could be used to measure accurately small temperature differences. The proximity effect near a node and the equivalence of the nonlinear solutions of the above circuit with circuits of different geometries and transport or shielding currents are discussed.

I. INTRODUCTION

It was shown[1] recently that a superconducting ring of homogeneous wire of transverse dimensions smaller than ξ and λ and uniform cross section, connected to two long leads, should, for appropriate ring sizes, behave like a superconducting quantum interference device (SQUID) in the presence of an external current and applied magnetic field. ξ and λ are the temperature-dependent Ginzburg-Landau (GL) coherence length and penetration depth. This prediction is based on the nonlinear adaptation of the de Gennes–Alexander[2–4] approach to uniform micronetworks. This work gives not only a detailed account of the micro-SQUID but also investigates, in general, the behavior of the order parameter along three branches connected to a node in the presence of currents. When applied to the SQUID below, two of the branches are of equal (not necessarily) and finite length, the other is very much larger than $\xi(t)$. A node with three connecting wires carrying currents is the basic structure for many nets topologically similar to the SQUID (e.g., the ladder[5]). The fluxoid quantization relation joins together external transport currents with persistent currents in a multiple connected superconducting network or array due to the presence of magnetic flux.

Previous nonlinear calculations involving currents in micronets or in elements of micronetworks are the following. The diamagnetic properties of the lasso[2] due to persistent currents were obtained by Straley and Visscher,[6] critical transport current densities in long superconducting wires with dangling side branches were calculated in Ref. 7, and critical applied current densities for wire arrays in zero applied magnetic fields are published in Ref. 8. The present work which combines applied and persistent currents and magnetic flux goes far beyond the results of Refs. 6–8.

Section II outlines the general nonlinear theory of micronetworks as applied to the SQUID, Sec. III is a short summary of the numerical procedures as used in obtaining the present results, and Sec. IV summarizes the numerical results for three external measuring (transport) current densities (J). One of the latter is very close to the critical current density (J_c) of a very long superconducting wire, one is about $0.5J_c$ and the other is very much smaller than J_c. There are interesting, but esoteric, differences in the results between $J \ll J_c$ and $J=0$ which will be discussed elsewhere. Section V is devoted to the conclusions.

II. GENERAL THEORETICAL FRAMEWORK

In conventional units the GL equations are (see, e.g., Ref. 9)

$$\xi^2\nabla^2 f=(f^2+q^2-1)f \ , \tag{1}$$

$$f^2\mathbf{q}=(4\pi/c)(2\pi\xi\lambda^2/\phi_0)\mathbf{J}_{\rm conv}\equiv J \ , \tag{2}$$

where $f(r)$ is the modulus of the complex order parameter $\Psi=f\exp[i\theta(r)]$ and $J_{\rm conv}$ is the conventional current density in cgs Gaussian units (statamperes/cm^2). The superfluid velocity is

$$\mathbf{q}=\xi(\nabla\theta-2\pi\mathbf{A}/\phi_0) \ , \tag{3}$$

where $\mathbf{A}$ is the vector potential, ϕ_0 is the fluxoid quantum $ch/2e$, ξ is the temperature-dependent bulk coherence length, and λ is the temperature-dependent bulk penetration depth.[10] The function f^2 is proportional to the superfluid number density and it is unity when the current density and magnetic field are zero.

For our problem it is assumed that the distance between the nodes are of order of magnitude of $\xi(t)$ and that the wire diameter $2a<\lambda(t)$ and $\xi(t)$. Then the one-dimensional GL equations may be used with x being the curvilinear coordinate along the wire normalized by $\xi(t)$. When the superfluid velocity in the first GL equation is eliminated in terms of the normalized supercurrent density J by use of the second GL equation, the result in normalized form is

$$\frac{d^2f}{dx^2}+(1-f^2-J^2/f^4)f=0 \ , \tag{4}$$

 ©1988 The American Physical Society

where $f=f(x)$ and J is a constant. Integrating Eq. (4) once and substituting for $f^2(x)=f_0^2+t^2(x)$, where f_0 is the absolute value of the order parameter at some extremum of $f(x)$, one obtains

$$2f^2\left[\frac{df}{dx}\right]^2=(f_0^2-f^2)[f^2(2-f_0^2-f^2)-2J^2/f_0^2] \quad (5)$$

or

$$\left[\frac{dt}{dx}\right]^2=J^2/f_0^2-f_0^2(1-f_0^2)-(1-3f_0^2/2)t^2+t^4/2 \ . \quad (5')$$

The function $t(x)$ gives rise to the modulation of the absolute value of the order parameter. It is zero at the extremum where $f(x)=f_0$. We assume that the material throughout the network is the same and homogeneous so that $f(x)$ is continuous at each node. In addition, complex current conservation[4] requires that at all nodes

$$\sum\left[\frac{i\partial\Psi_n}{\partial x}+\frac{2\pi A\Psi_n}{\phi_0}\xi\right]=0 \quad (6)$$

are satisfied. Here A and Ψ_n are, respectively, the vector potential along the wire and the complex order parameter at node n, and the sum is over all branches connected directly to node n.

From the real and imaginary parts of Eq. (6), one finds the following subsidiary conditions at the nodes:

$$\sum\left[\frac{d\theta_n}{dx}-\frac{2\pi A}{\phi_0}\xi\right]\equiv\sum q_n=0 \ , \quad (7)$$

$$\sum\frac{df}{dx}=0 \ , \quad (8)$$

where q_n is the superfluid velocity entering the node, and the derivatives of $f(x)$ with respect to x are taken radially outward from the node. Equation (7) is equivalent to Kirchhoff's current law. Equation (8) is an additional constraint for superconducting networks.

The fluxoid relation, obtained from a contour integration of the second GL equation, Eq. (2), is

$$n\phi_0=\phi+\frac{\phi_0}{2\pi}\oint\frac{\mathbf{J}\cdot d\mathbf{x}}{f^2(x)} \ , \quad (9)$$

where n is a positive or negative integer or zero and ϕ is the internal (total) magnetic flux enclosed by the contour. Note that x is normalized by $\xi(t)$ in Eq. (9).

Consider the ring circuit shown in Fig. 1. The internal flux as a function of the applied (external) flux ϕ_a and the persistent circulating current $I(\phi)$ (Gaussian units) is

$$\phi=\phi_a+(1/c)LI(\phi) \ , \quad (10)$$

where L is the self-inductance of the loop. In order for the second term on the right-hand side (rhs) to be physically meaningful, the wire of the loop must have a finite cross-sectional area of radius a. Then the current $I(\phi)=\pi a^2 J_{\rm conv}$ should be interpreted as the net circulating current in the ring (I_B).

In the same spirit as Eq. (9) was obtained, the general expression for the phase difference $\Delta\theta$ between two points in a superconductor is given by

$$\Delta\theta=\frac{4\pi}{c}\lambda^2\frac{2\pi}{\phi_0}\int_1^2\frac{\mathbf{J}_{\rm conv}\cdot d\mathbf{x}}{f^2}+\frac{2\pi}{\phi_0}\int_1^2\mathbf{A}\cdot d\mathbf{x} \ , \quad (11)$$

where $J_{\rm conv}$ is the total local current density.

In the bulk of a massive superconductor the contribution due to the first term on the right-hand side of Eq. (11) is negligible. However, at a weak link the value of f can be made very small and this is the origin of the weak link's dephasing properties.

We are interested in the general case where both a transport current density J and a circulating current density J_B, created by the magnetic flux difference of Eq. (10), are present. This circuit is shown in Fig. 1 and J_B is related to the current $I(\phi)$ in Eq. (10). For given sets of values of R/ξ, J, and J_B we have found exact numerical solutions of $f(x)$ (shown in the figures) which satisfy Eqs. (4)–(8) along the wire with $\Psi(x)$ continuous along the whole circuit.

Also of interest is the relation between the circulating current density J_B and the magnetic flux for a fixed measuring current density. This is obtained by integrating Eq. (11) along the complete circuit which gives

$$2\chi=\Delta\theta_1+\Delta\theta_2=(2J_B+J)\,|\,C_1\,|+(2J_B-J)\,|\,C_2\,| \ , \quad (12)$$

where $\chi=\pi(n-\phi/\phi_0)$ and

$$C_1=\int_{f_{01}}^{f_N}dx/f^2, \quad C_2=\int_{f_{02}}^{f_N}dx/f^2 \ .$$

Here the appropriate values for the current densities are $J/2+J_B$ along branch 1 and $J/2-J_B$ along branch 2.

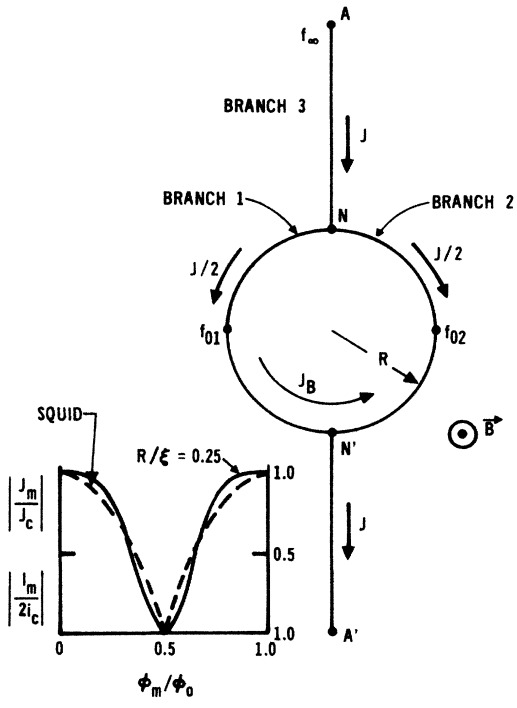

FIG. 1. Schematic diagram of circuit which is analyzed in this work and notation used. Inset shows schematic results of Ref. 1.

The extreme values of f on each branch are f_{01} and f_{02} as shown in Fig. 1. Using the results of our computations, we have evaluated Eq. (12) numerically for different sets of values of R/ξ, J, and J_B. The angle δ imposed by the measuring current across the SQUID as a function of ϕ for the same value of $J/J_c = I/I_c$ is defined by

$$2\delta = \Delta\theta_1 - \Delta\theta_2 , \tag{13}$$

where $\Delta\theta_1 = (2J_B + J)\,|\,C_1\,|$ and $\Delta\theta_2 = (2J_B - J)\,|\,C_2\,|$.

III. NUMERICAL PROCEDURES

The solution of the order parameter

$$f(x) = [f_0^2 + t^2(x)]^{1/2} \tag{14}$$

was obtained from Eq. (5). The value of $f(x)$ at some extremum is f_0 and $t(x)$ is one of the Jacobian elliptic functions which are periodic. The period is $4K$ where K is the complete elliptic integral. The solutions of Eq. (5) depend on the current density in the wire, on the length of the branch, and on the value of f_0. As can be seen from Fig. 1, because of symmetry, at points halfway between nodes N and N', the order parameter will be an extremum, f_{01} on branch 1 and f_{02} on branch 2. Since it is assumed that the distance $\overline{AN}$ is very much larger than the coherence length $\xi(t)$, the order parameter at point A, f_∞, is also assumed to be an extremum. The current density J due to the external source current is then related to f_∞ by [see, e.g., Eq. (4) with $d^2f/dx^2 = 0$]

$$J = f_\infty^2 (1 - f_\infty^2)^{1/2} . \tag{15}$$

The applicable current densities are $(J/2 + J_B)$ in branch 1, $(J/2 - J_B)$ in branch 2, and J in branch 3.

As input parameters to our program we use R/ξ, J_B, and f_∞ (which determines J). Applying Eq. (5) to branch 3, a relation results between the slope $(df/dx)_3$ and $f_3(x) = f_{n_3}$ at node N if for f_0 the value f_∞ is substituted and for $J^2 = f_\infty^4 (1 - f_\infty^2)$. Similarly for branch 1 [2], we guess some value $f_0 = f_{01}$ [f_{02}] and substitute it into the various Jacobian elliptic functions and replace in those functions J by the value $(J/2 + J_B)$ [$(J/2 - J_B)$] and obtain, for a fixed ring radius, the slope at $(df/dx)_1$ [$(df/dx)_2$] on branch 1 [2] and the value of $f_1(x) = f_{n_1}$ [f_{n_2}] at node N. We then proceed in the following way: We let $f_{n_3} = (f_{n_1} + f_{n_2})/2$, substitute f_{n_3} in the above relation for branch 3, and then test

$$f_{n_1} - f_{n_2} = \varepsilon_1 \tag{16}$$

and Eq. (8), taking into account that the derivatives of $f(x)$ with respect to x are to be taken radially outward from the node

$$\pm(df/dx)_1 \pm (df/dx)_2 \pm (df/dx)_3 = \varepsilon_2 . \tag{17}$$

In order for a solution to be acceptable, both ε_1 and ε_2 must approach zero. Of course, this depends on the correct choice of the values of f_{01} and f_{02}. We, therefore, divide the f_{01}-f_{02} plane into a fine grid and test the various points of the grid for ε_1 and ε_2. Once acceptable values of ε_1 and ε_2 are found for a solution with the largest possible period, the f_{01}-f_{02} plane around this point is further divided into a finer grid and the solution is tested again to obtain refined values of f_{01} and f_{02} until $|\,\varepsilon_1\,|$ and $|\,\varepsilon_2\,|$ are smaller than 0.000 001. Then the magnetic flux parameter $\chi = \pi(n - \phi/\phi_0)$ and the phase difference between the nodes N and N', δ, are calculated from Eqs. (12) and (13).

IV. NUMERICAL RESULTS

The insert of Fig. 1 shows schematically the maximum measuring current density of J, J_m, as a function of the corresponding magnetic flux ϕ, ϕ_m, for $R/\xi = 0.25$ as shown in Ref. 1. This curve is compared with that of a conventional SQUID calculated with $\delta = \pi/2$ and $n = 0, 1$ from

$$I_m/2i_c = \cos\chi . \tag{18}$$

In each case the curves are normalized by the intrinsic critical current (density) of the whole device, that of an infinitely long wire J_c for the above ring circuit, and by $2i_c$ for the conventional symmetric SQUID, where i_c is

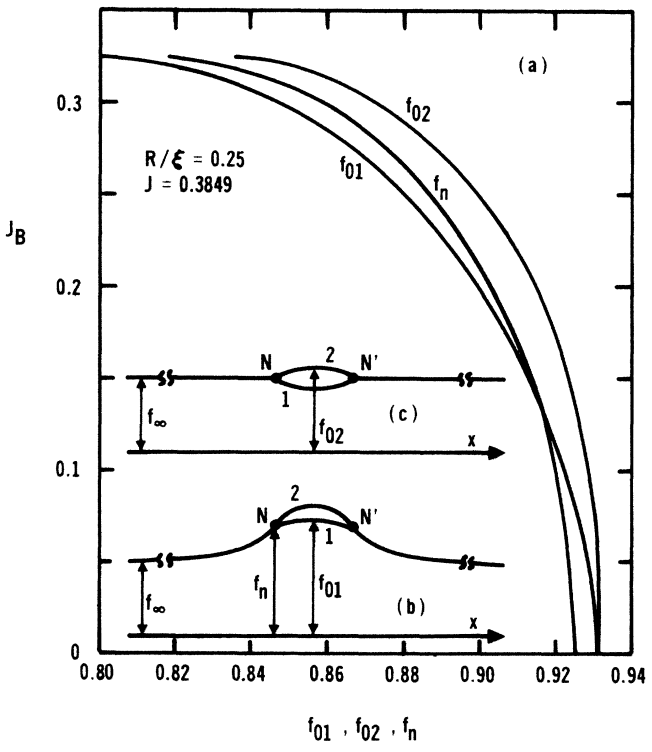

FIG. 2. (a) Persistent current density J_B as a function of the absolute value of the order parameter at node N (or N'), f_n, and halfway between N and N', f_{01} and f_{02}, where the order parameters are extrema. The normalized measuring current density $J = 0.3849$ is slightly less than J_c and the ring radius is $\xi/4$. For notation see Fig. 1. (b) Schematic of order parameter $f(x)$ between A and A' (see Fig. 1) for $J_B \lesssim 0.1$ and for (c) $J_B = 0.324$.

the critical current of each Josephson junction (JJ). As can be seen, the ring without *JJ*'s for values of $R/\xi=0.25$ has a phase boundary between the fully superconducting and finite resistance states that is very similar to that of a conventional SQUID. However, as shown in Ref. 1, that similarity depends strongly on $R/\xi(t)$.

Here we shall show our general results for various values of ring radii for external current densities J at the critical value J_c, for $J \ll J_c$, and about halfway between. The following values of measuring currents were used: $J/J_c=1.000\,00$, 0.496 54, 0.025 98 with $J_c=2/\sqrt{27}$. For each curve shown, the external current density J and the normalized ring radius R/ξ are kept constant. Shown is the normalized circulating current density J_B as a function of the order parameters at the extrema f_{01}, f_{02} and at the node f_n, the circulating current density as a function of the internal flux ϕ, normalized by the fluxoid quantum ϕ_0, and the phase difference δ between the nodes N and N' due to the measuring current density J. If the self-inductance L of the ring is known, the applied flux ϕ_a can be obtained from $\phi=\phi_a+LI_B/c$.

Figure 2(a) shows the relation between the order parameters and the circulating current J_B for $J=0.384\,90$. As input to our program the value $f_\infty=0.816\,500$ was used. This value is $\sqrt{2/3}-0.000\,003$, very close to the critical value. Figures 2(b) and 2(c) show schematically the spatial dependence of $f(x)$ along the various branches, (b) for $J_B\simeq 0.05$ and (c) for $J_B=0.324$. For $J_B=0$ the solutions along branches 1 and 2 are maxima and of the same value (symmetric). As J_B increases, f_{01} decreases more rapidly than f_{02}, becomes equal to f_n for $J_B\simeq 0.145$, and then becomes a minimum for $J_B>0.145$ and $f_n>f_\infty$. As J_B increases further the slope of branch 3 at N becomes zero when $f_n=f_\infty$. A further increase of J_B makes the right-hand side of Eq. (5) negative, $(df/dx)_3$ becomes imaginary, and there is no real solution for $f_n<f_\infty$ for the above value of the measuring current density J.

This cutoff occurs only for J values in the neighborhood of J_c and is also R dependent. For $R/\xi\geq 1.5$ there is no cutoff. For $1.5>R/\xi\geq 0.5$ the cutoff occurs on the left-hand side (lhs) of the J_B maximum (see Fig. 5 for an equivalent description of the maximum) and for $R/\xi\leq 0.25$ the cutoff occurs on the "right-hand side" of the virtual maximum of J_B. It can be proven that the condition for cutoff is reached when f_n has decreased to a value given by

$$f_n=[2(1-f_\infty^2)]^{1/2} \tag{19}$$

at which point the slope of branch 3 at the node becomes zero and a further decrease of f_n makes $(df/dx)_3$ imaginary [the rhs of Eq. (5) changes sign]. For $J<J_c$ the value of $(df/dx)_3$ also becomes zero when $f_n=f_\infty$ as is obvious from Eq. (5). However $(df/dx)_3^2$ does not change sign at this point as f_n becomes smaller than f_∞ as J_B is changed until Eq. (19) is satisfied.

Figures 3 and 4 show the circulating current J_B and the phase difference between N and N' as a function of the enclosed magnetic flux for the same measuring current as used in Fig. 2. It is obvious from Fig. 3 and the insert of Fig. 1 that for $R/\xi\gtrsim 1.35$ the dc quantum interference effect ceases to work properly since for different quantum numbers the maximum and minimum fluxes ϕ_m at $\phi/\phi_0=\frac{1}{2}$, and $n=0$ and 1 are overlapping and $dI_m/d\phi_m$ becomes zero (see Ref. 1). For the smaller

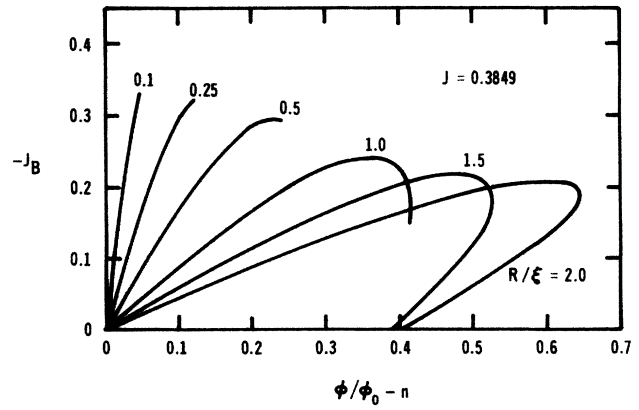

FIG. 3. Persistent current density J_B as a function of flux ϕ enclosed by the ring circuit for various ring radii R for the same measuring current density J as used in Fig. 2.

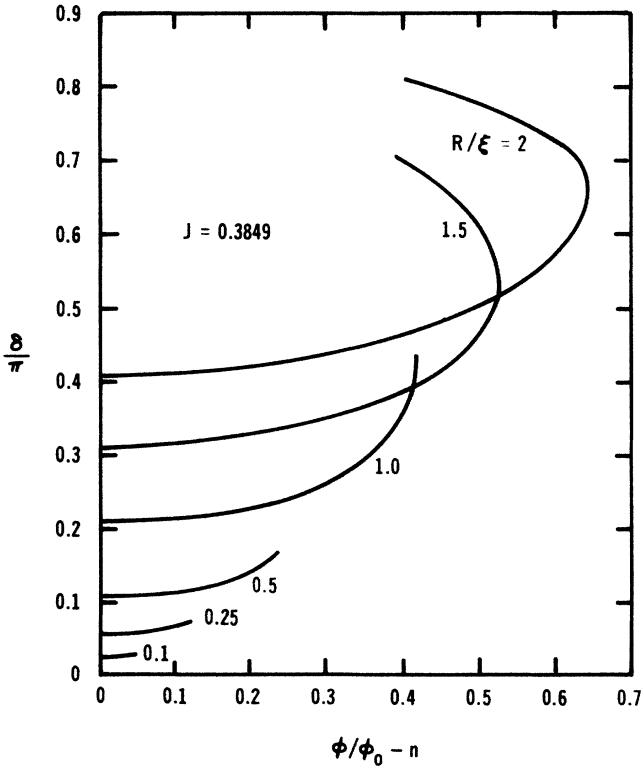

FIG. 4. Phase-shift δ imposed by J across the circuit between N and N', Eq. (13), as a function of flux ϕ enclosed by the ring for various ring radii. The value of J is the same as in Figs. 2 and 3.

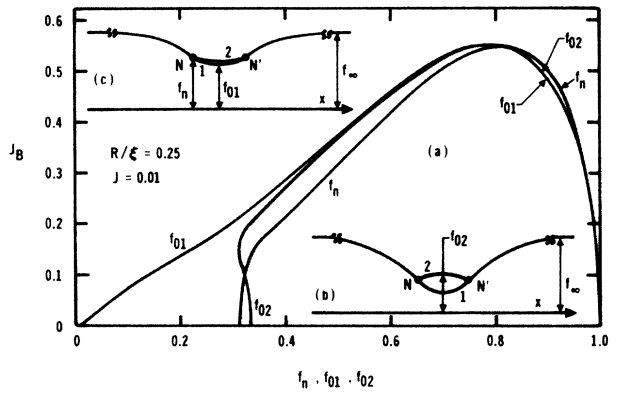

FIG. 5. (a) Similar plot as Fig. 2 except that the measuring current $J=0.01$ ($\ll J_c=2/\sqrt{27}$). (b) Schematic of $f(x)$ between A and A' (see Fig. 1) for $J_B<0.103$ and $f_n<0.325$ while (c) applies to the rest of the figure except when f_n is near unity where Fig. 2(b) applies.

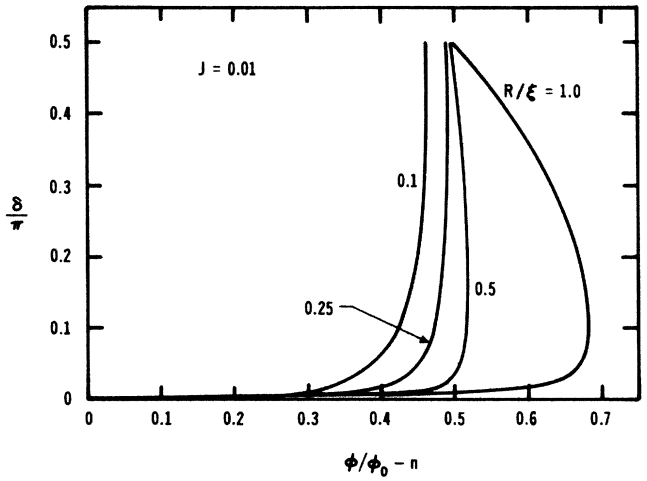

FIG. 7. Similar to Fig. 4 except J is the same as in Figs. 5 and 6.

radii a "normal" region in the vicinity of $\phi/\phi_0-n=0.5$ appears which becomes larger as R/ξ is decreased. As was shown in Ref. 1 for $R/\xi=0.25$, the phase boundary between the zero resistance and resistive states for our circuit is very similar to that of the conventional SQUID. As R/ξ decreases below the value of 0.25 the normal region widens near $\phi/\phi_0-n=0.5$ so that for very small radii the ring circuit would always be in the normal state for values of the flux ϕ/ϕ_0 near $\pm\frac{1}{2}$, $\pm\frac{3}{2}$, etc.

Figures 5 to 7 show the behavior of our circuit on the opposite side of the measuring current scale, that is, for

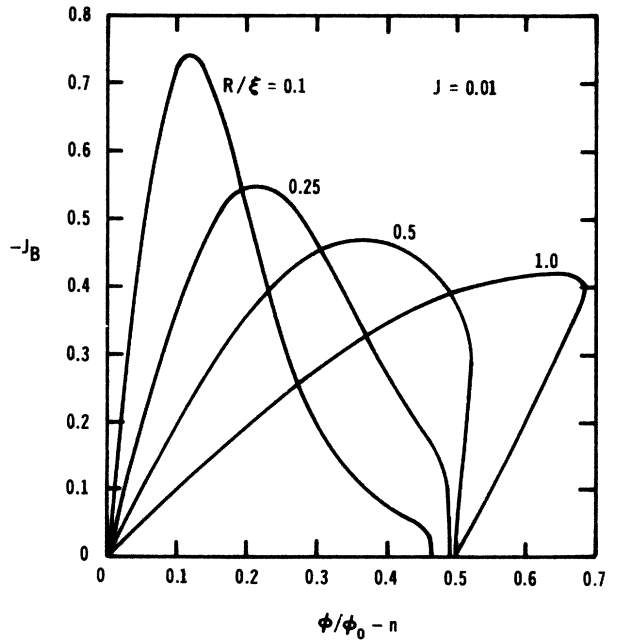

FIG. 6. Similar to Fig. 3 except J is the same as in Fig. 5.

$J=0.01$ ($f_\infty=0.999\,95$). Figure 5(a) shows the relation between the circulating current J_B and the order parameters f_{01}, f_{02}, and f_n.

The spatial dependence of the order parameters along the various branches are shown schematically in Figs. 5(b) and 5(c). Figure 5(b) is a schematic plot for $J_B<0.103$ and $f_n<0.325$ while Fig. 5(c) is representative of the rest of Fig. 5(a) with the exception of $f(x)$ values very near unity where the behavior of $f(x)$ is very similar to that shown in Fig. 2(b). Although not visible in the plot, $f_n<f_{01}$ and f_{02} near unity.

The crossover point between f_n and f_{02} for small values of $f(x)$ shift to larger values of J_B for larger values of R/ξ. For example, for $R/\xi=0.5$ the crossover occurs at $J_B\simeq 0.321$ ($f_n\simeq 0.650$), and for $R/\xi=1.0$ at $J_B\simeq 0.387$ ($f_n\simeq 0.842$).

Figure 6 is similar to Fig. 3 except that the measuring current density J is small. For the values of R/ξ shown, there exists no cutoff of the solutions as it does for the larger measuring current densities and smaller R/ξ values. For $R/\xi=0.5$, for example, the largest flux ϕ_m exceeds $\phi_0/2$ (e.g., for $n=0$) for small values of the measuring current density J ($\lesssim 0.01$), while for J near the critical current the same value of R/ξ has a value of $\phi_m\approx 0.241\phi_0$. This is, of course, the property which is exploited by a dc quantum interferometer as shown in the insert of Fig. 1 and explained in Ref. 1.

Figure 7 shows the phase difference δ across the SQUID between nodes N and N' (Fig. 1) as a function of flux which is locked-in within the ring circuit. Contrary to what is shown for large measuring current densities J in Fig. 4, for small values of J there is not much change of δ for small values of ϕ. Appreciable changes of δ occur only when $\phi\approx\phi_0/2$ (e.g., for $n=0$) and $\delta\rightarrow\pi/2$ when J_B (Fig. 6) approaches zero there. As can be seen from Fig. 4, for large measuring current densities J, the value of δ is appreciable at $\phi=0$ while for $J\ll J_c$ the value of δ is very small at $\phi=0$.

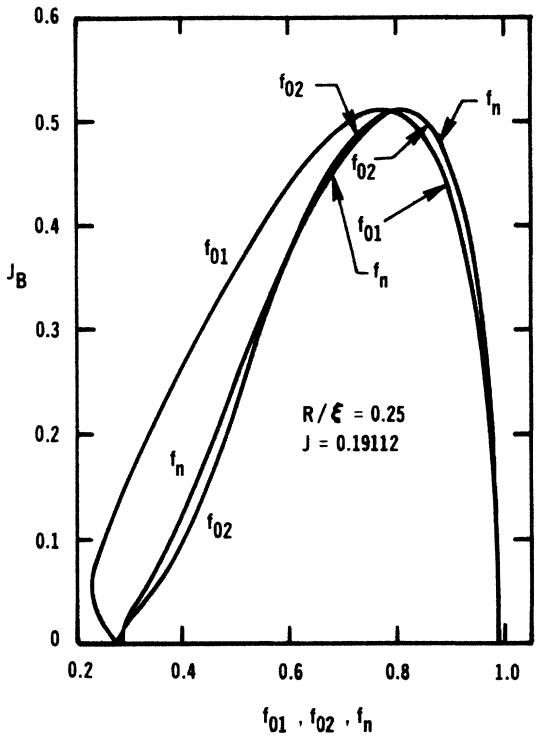

FIG. 8. Similar plot as in Fig. 2 except that the normalized measuring current density $J \approx 0.5 J_c$.

To complete the picture, plots similar to those shown in Figs. 2–7 are shown for measuring currents approximately halfway between those shown above. Figures 8–11 are for $J = 0.191\,12$ ($f_\infty = 0.98$). Figure 8 shows the relations between J_B and the order parameters f_{01}, f_{02}, and f_n for $R/\xi = 0.25$. In the vicinity where $J_B \ll J_c$ and $f(x)$ is near unity, the spatial dependence of the order parameters is similar to that shown in Fig. 2(b). The schematic shown in Fig. 5(b) is typical of J_B values near 0.2 on the left-hand side of the maximum, and Fig. 5(c) is a schematic representation for $J_B \simeq 0.47$ and larger on both sides of the maximum of J_B.

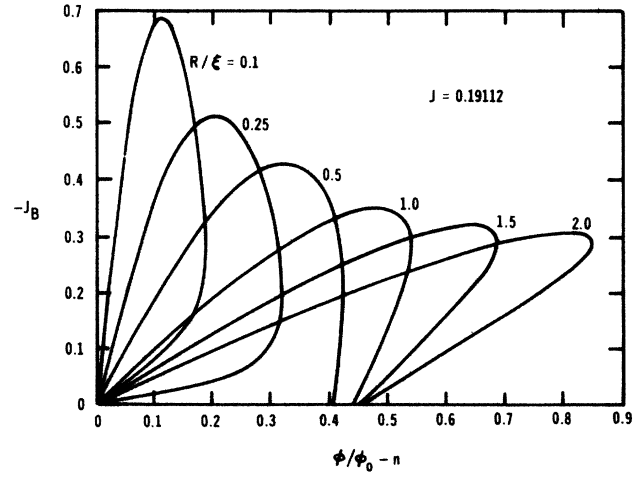

FIG. 9. Similar to Fig. 3 except J is the same as in Fig. 8.

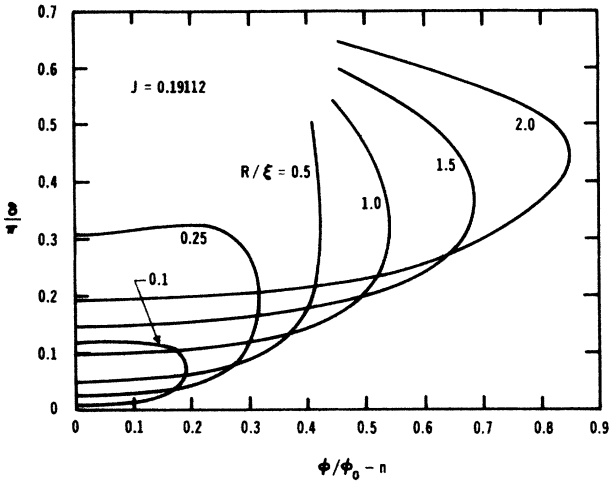

FIG. 10. Similar to Fig. 4 except J is the same as in Figs. 8 and 9.

For this and smaller R/ξ values there exist symmetric solutions for $f(x)$ at $J_B = 0$ on the left-hand side of the maximum. In our case $f_{01} = f_{02} \simeq 0.28$ at $J_B = 0$. It was demonstrated (see also Fig. 11) that the symmetric solution ceases to exist for R/ξ somewhere in between $R/\xi = 0.35$ and 0.4.

Figures 9 and 10, which are similar to Figs. 3, 4, 6, and 7, but for $J = 0.191\,12$, show the transition from the symmetric to the asymmetric solution for the smaller f_{01} and f_{02} values by the closed and open curves as R/ξ is changed. Figure 11 is similar to Fig. 8 except that

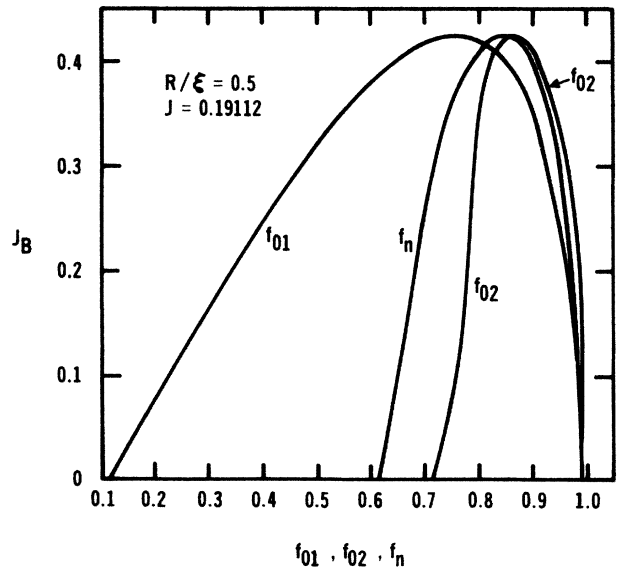

FIG. 11. Similar plot as in Fig. 8 except that the ring radius $R = \xi/2$.

$R/\xi=0.5$. The asymmetric solution on the left-hand side of the J_B maximum for $J_B=0$ is apparent. Thus a large variety of $f(x)$ and related functions are possible as the measuring current, the flux and the ring radius are varied. This property leads to useful applications such as a dc quantum interference device.[1]

V. CONCLUSIONS

As shown by the insert of Fig. 1 and our present analysis the device described here can be used for dc measurements in much the same way as an ordinary SQUID with Josephson junctions provided the radius of the ring is of order of magnitude of $\xi(t)$. In addition, because of the temperature variation of ξ, our circuit has the versatility that its normal- (N) superconducting (S) phase boundary can be modified with temperature. This property modulates the NS phase boundary with temperature and could lend itself to accurate measurements of small temperature differences. For details of the phase boundary see Fig. 2 of Ref. 1.

We conclude further: When the measuring current in the SQUID is subdivided at node N into branches 1 ($B1$) and 2 ($B2$) and there is no circulating current I_B, $B1$, and $B2$ have the tendency to enhance superconductivity (increase of number density of Cooper pairs) near the node in branch 3 ($B3$). This happens also when the circulating current is small compared to the measuring current. In that case the current carried by $B1$ and $B2$ is about one-half the current in $B3$ and this depresses superconductivity less strongly between N and N' than in $B3$ (see Fig. 1). Because of the reduced currents in the circular branches and nodal condition, Eq. (8), the order parameter $f(x)$ has a maximum in $B1$ and $B2$ while in $B3$ it has a minimum. The relative amount of aid received by $B3$ near N depends also on the lengths of $B1$ and $B2$. If the latter are much shorter than $\xi(t)$ the aid given to $B3$ is smaller than when the lengths of $B1$ and $B2$ are comparable to or larger than 2 to 3 $\xi(t)$. When the branches are much larger than $\xi(t)$, the enhancement does not increase by a significant amount since this proximity effect extends spatially over a distance of about $\xi(t)$ from the node.

When a persistent current I_B is flowing in addition to the transport current I, comparable in magnitude to I, the amount of superconductivity in $B1$ is reduced considerably relative to that in $B2$ because in the former the total current is $I_B+I/2$ while in the latter it is $I_B-I/2$. So a minimum of $f(x)$ is created in $B1$ while $B2$ contains a maximum.

When, however, I is small compared to I_B, both branches will contain a minimum of $f(x)$ while in $B3$ there is a maximum of $f(x)$. Thus the reverse happens as above, namely $B3$ enhances superconductivity in $B1$ and $B2$ near the node since near point A, that is far from N, $f(x)$ in $B3$ reaches a maximum value (the almost fully superconducting state).

Thus the relative aid a branch receives (provides) in enhancing the amount of superconductivity from (to) the neighboring branches depends in a complicated way on the currents in the various branches and their lengths. One can state that a branch with the largest maximum value of $f(x)$ will aid the other branches in increasing the amount of superconductivity near a node.

The above numerical results for the SQUID can also be adopted to a number of different situations. For example, the SQUID without a transport current ($J=0$) is symmetric in $f(x)$ along $B1$ and $B2$ ($f_{01}=f_{02}$). One can imagine then that joining the two branches together at their minima leads to a lasso with a long arm. Then the numerical solutions of the SQUID of radius R are equivalent to those of a lasso[6] with radius equal to $R/2$. The above program can be modified easily to obtain results for a lasso with any arm length.

Similarly, a wire with dangling side branches and a transport current[7] through it can be simulated by a SQUID with $J=0$. Then the circulating current takes on the function of the transport current in the wire and the minimum of $f(x)$, located halfway between the nodes, distance a apart, has the value $f(a/2)=f_{01}=f_{02}$.

Equally, the nonlinear solution of the ladder[5] with shielding currents only (no vortex currents, wave vector $q=0$) can be simulated by the above SQUID solutions with $J=0$ and $J_B\neq 0$ or by the nonlinear solution of a wire with finite dangling branches.[7] Arrays with transport currents in zero applied magnetic field[8] can also be obtained from the above SQUID solutions by similar considerations.

ACKNOWLEDGMENTS

This project was supported in part by the National Science Foundation (NSF) through Grant Nos. ECS-8505627 and INT-8502375. Enlightening discussions with A. López and V. Grünfeld are acknowledged.

---

*Present address: Department of Electrical and Computer Engineering, University of California, Santa Barbara, CA 93106.
†Present address: Revelle College, University of California, San Diego, CA 92093.

[1] H. J. Fink, V. Grünfeld, and A. López, Phys. Rev. B **35**, 35 (1987); H. J. Fink, J. Loo, and S. M. Roberts, Jpn. J. Appl. Phys. **26**, Suppl. 26-3, 1605 (1987).
[2] P. G. de Gennes, C. R. Acad. Sci., Ser. II **292**, 279 (1981).
[3] S. Alexander, Phys. Rev. B **27**, 1541 (1983).
[4] H. J. Fink, A. López, and R. Maynard, Phys. Rev. B **26**, 5237 (1982).
[5] J. Simonin, D. Rodrigues, and A. López, Phys. Rev. Lett. **49**, 944 (1982).
[6] J. P. Straley and P. B. Visscher, Phys. Rev. B **26**, 4922 (1982); H. J. Fink and V. Grünfeld, *ibid.* **33**, 6088 (1986).
[7] H. J. Fink and V. Grünfeld, Phys. Rev. B **31**, 600 (1985).
[8] H. J. Fink and A. López, J. Phys. (Paris) Lett. **46**, L961 (1985).
[9] M. Tinkham, *Introduction to Superconductivity* (McGraw-Hill, New York, 1975).
[10] In the figures which follow, the magnetic flux is plotted in

units of $\phi_0=2.07\times10^{-7}$ G cm^2, and the circulating and measuring current densities in units of $(\phi_0/2\pi)[c/4\pi\xi(t)\lambda^2(t)]$ [see Eq. (2)]. For example, for indium, for which $\xi(0)\approx0.18\times10^{-4}$ cm and $\lambda(0)\approx1.6\times10^{-6}$ cm the latter normalization constant at 0 K is equal to 1.7×10^{18} statampere/cm^2 or 5.7×10^8 A/cm^2. Since the largest J's (J or J_B) in the figures are of order of unity, the conventional current densities are of order of 10^8 A/cm^2 at 0 K. This is of the same order of magnitude as the shielding current densities in the Meissner state.